Please cite as

G. Di Martino, A. Iodice, “Passive beamforming with coprime arrays”, *IET Radar Sonar Nav.*, vol. 11, no. 6, pp. 964-971, June 2017. DOI: 10.1049/iet-rsn.2016.0517.

Passive Beamforming with Coprime Arrays

Gerardo Di Martino*, Antonio Iodice

DIETI, Università di Napoli Federico II, 80125, Napoli, Italy
*gerardo.dimartino@unina.it

Abstract: Coprime arrays have been recently proposed as effective sparse configurations suitable for radar beamforming and angle-of-arrival estimation applications. In this paper, a new approach for passive beamforming using coprime arrays is presented. In particular, a new detection strategy is proposed, which outperforms the coprime processors presently available in the literature, both in terms of peak sidelobe ratio and integrated sidelobe ratio, without giving rise to "ghost" targets in presence of multiple interferers. The advantage of the proposed detector is demonstrated through the simulation of appropriate array scanned responses and receiver operating characteristic (ROC) curves.

1. Introduction

The significant advances in millimeter-wave technology and radar applications, along with the restless search for high resolution, are the driving factors of a renewed interest in the field of sparse array structures. Indeed, the reduction of the number of elements of an array has positive effects in lowering the complexity of the physical structure and of its calibration, and in decreasing the overall system processing requirements. Moreover, sparse arrays also mitigate the effects of mutual coupling between the elements, due to the larger inter-element spacing.

Recently, the concept of coprime arrays was introduced as an effective solution for sparse sensing in active and passive scenarios [1-8]. They are based on the combined use of two sub-arrays obtained undersampling a uniform linear array (ULA) with two coprime integer factors. The difference co-array [7-8] generated from the two coprime sub-arrays holds an increased number of degrees of freedom that can be exploited in angle of arrival (AoA) estimation problems [4-6] and radar beamforming applications [1]. From the viewpoint of antenna-array theory, the advantages of coprime arrays are related to the fact that the grating lobes of the two sparse arrays are never located at the same azimuth angle, thanks to the coprimality of the two undersampling factors. Essentially, they can be considered as thinned arrays, for which very high thinning factors can be obtained [11]. However, especially in passive radar beamforming scenarios [10-11], signal detection requires ad hoc processing architectures. In particular, in [1] it was proposed to use snapshot time averages of the product of the output signals of the two sub-arrays to filter out the contributions due to the grating lobes. With this architecture, which we call product detector, it is possible to strongly reduce grating lobes' levels. However, rather high sidelobes' levels remain. Another kind of coprime detector was firstly proposed by the authors in [7] for SAR applications, and it was then considered for more general beamforming scenarios in [8], where it was named the min detector. This

detector has the relevant advantage of significantly reducing the sidelobe levels with respect to the product detector case.

In this paper, we develop a different architecture for coprime-array signal detection, which inherits the benefits of each of the abovementioned detectors, without the associated drawbacks. In particular, we show that the proposed processing is able to solve critical "ghost" target issues experienced by the min detector in presence of multiple interferes arriving from the grating lobes of both sub-arrays. Moreover, we show that the proposed architecture is able to outperform both the product processor [1] and the min processor [8] in terms of peak sidelobe ratio (PSLR) and integrated sidelobe ratio (ISLR). Several scenarios, including interferers placed in critical locations, are discussed through the simulation of appropriate array scanned responses. Finally, comparison of proposed and available detectors' performances is carried out in terms of probability of detection (PoD) and false alarm rate (FAR) for different values of signal-to-noise ratio (SNR), and both in the absence and in the presence of interferers.

2. Theoretical background

A coprime array consists of two sub-arrays obtained undersampling a ULA made up of cMN elements with two factors N and M (we assume $N<M$), where N and M are coprime integers, and c is an arbitrary integer. The inter-element spacing of the two sub-arrays will be $N\lambda/2$ (array 1, made up of cM elements) and $M\lambda/2$ (array 2, made up of cN elements), respectively, where λ is the considered electromagnetic wavelength. The coprime array can be obtained interleaving the two sub-arrays so that they share the first element, as shown in Fig. 1. The obtained array is a sparse non-uniform linear array, made up of $c(M+N-1)$ elements with total aperture size equal to $cM(N-1)\lambda/2$. Therefore, being the aperture size of the array comparable to that of the initial ULA, the width of the main beams of the two arrays will be comparable.

Since their inter-element spacing is larger than $\lambda/2$, the radiation patterns of the two sub-arrays will present grating lobes. In particular, the normalized patterns of the two sub-arrays are given by

$$f_1(u) = \frac{1}{cM}\frac{\sin\left(\frac{\pi cMN}{2}u\right)}{\sin\left(\frac{\pi N}{2}u\right)} \quad (1)$$

$$f_2(u) = \frac{1}{cN}\frac{\sin\left(\frac{\pi cMN}{2}u\right)}{\sin\left(\frac{\pi M}{2}u\right)} \quad , \quad (2)$$

where $u = \sin\vartheta$ and ϑ is the azimuthal angle (see Fig. 1). Therefore, according to (1) the first sub-array will present grating lobes whenever $u = n\,2/N$, whereas the second one will have grating lobes for $u = m\,2/M$, with *n* and *m* relative integer numbers such that $|u| \leq 1$. However, due to the coprimality of *M* and *N*, the location of the grating lobes of the two sub-arrays will never coincide.

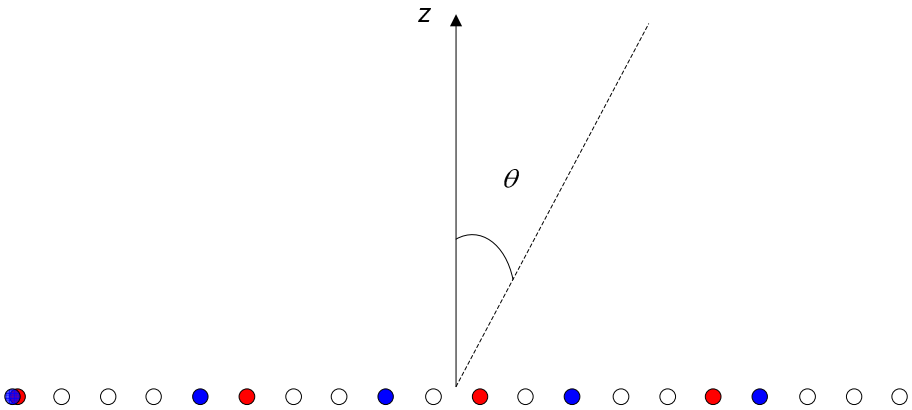

Fig. 1. *Geometry of the coprime array for c=1, N=4 and M=5. The elements of array 1 are represented in red, whereas those of array 2 are represented in blue. White circles represent the elements removed from the original ULA*

As demonstrated in [3], it is convenient to choose *M*–*N*=1 in order to minimize the total number of elements of the array [3]. In this case, the minimum distance between grating lobes of the two sub-arrays will occur for *n*=*m*=1, and it will be equal to 2/(*MN*). The nulls of the two patterns will be located at $u = \pm\,2/(cMN)$, i.e. at the same locations of those of the ULA. Moreover, the thinning factor TF of the coprime array, defined as the ratio between the number of elements removed from the full ULA and the number of elements of the ULA itself, is

$$\mathrm{TF} = 1 - \frac{2}{N} + \frac{2}{N(N+1)} \quad , \tag{3}$$

which for *N*>3, is greater than 0.5. Therefore, high TFs are attainable through coprime configurations.

The properties of the coprime array can be exploited in active beamforming for radar applications. In fact, if we use one of the two sub-arrays in transmission and the other one in reception, the signal contributions associated with the grating lobes of the transmitter's pattern are filtered out by the receiver's pattern. More specifically, the combined pattern will be given by the product of the sub-arrays' patterns

[1]. The only disadvantage is that the coprime array is vulnerable to jammers coming from the directions of the receiver's pattern grating lobes.

Conversely, in a passive radar scenario, the two sub-arrays are both used in reception and, in order to obtain grating lobes' rejection, an *ad hoc* processing has to be devised. In particular, two solutions have been proposed for detection. The original solution proposed in [1] consists in performing a time-average over suitable signal snapshots of the product of the output signal of the first sub-array by the complex-conjugate output signal of the second one, in order to reject the grating lobes' contributions of the two sub-arrays that are, indeed, poorly correlated. Thanks to this processing, it is possible to obtain a combined pattern equal to the product of the two patterns, similarly to the active beamforming case [1]. In addition, as we will verify in Section 3, this processing also allows for a good rejection of thermal noises over the two subarrays, which are poorly correlated as well. However, for c equal to unity, the PSLR of the product detector is rather poor, since its pattern presents sidelobe levels higher than those of the corresponding ULA, as shown in Fig. 2*a* for N=4 and M=5. This is due to the partial superposition of the grating lobes [3]. For this reason, for a given M and N pair, product-detected coprime arrays are convenient, at least in terms of PSLR, only for structures with aperture greater than $cMN\lambda/2$, where c is greater than unity. In [3] the minimum value of c (there called "extension factor") required for a coprime array to have a PSLR less than or equal to that of a full ULA was derived.

In Fig. 2*b* the pattern of the product-detected coprime array with extension factor c=3 is compared to the pattern of the corresponding ULA with equivalent aperture. It is evident that with this extension factor the PSLR of the product-detected coprime array is still about 3 dB higher than that of the corresponding ULA. A larger extension factor would be required to obtain lower sidelobe levels.

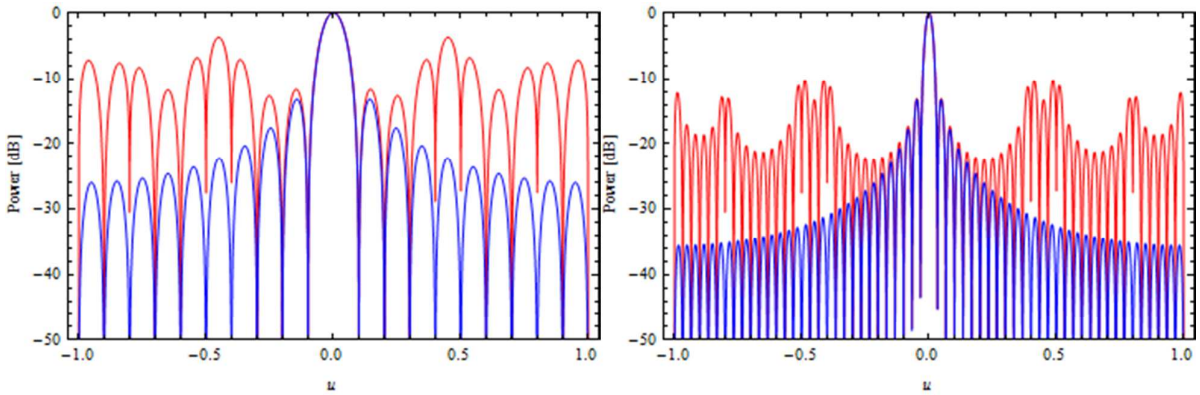

Fig. 2. *Pattern of the product-detected coprime array for N=4 and M=5, in red, compared with that of the ULA with cMN elements, in blue for*

a c=1, i.e., total number of elements of the coprime array is 8 and of the ULA is 20
b c=3, i.e., total number of elements of the coprime array is 24 and of the ULA is 60

Recently, we proposed a coprime configuration for Synthetic Aperture Radar, named CopSAR [7]. In particular, in [7] and [14] we used, as combination rule for the generation of the CopSAR image, the choice of the minimum value of the intensity between the two sub-images for each azimuth-range pixel. More recently, in [8] use of the min detector for coprime array beamforming was proposed. In this architecture, the minimum between the snapshot time averages of the output intensity of the two sub-arrays is chosen as output [8]. By using the min detector, it is possible to further reduce the sidelobe levels, as shown in Fig. 3, where it can be noticed that for the same coprime configuration considered in Fig. 2*b* both the PSLR and the ISLR significantly decrease. In particular, the PSLR of the coprime array has been reduced to the same value of the corresponding ULA.

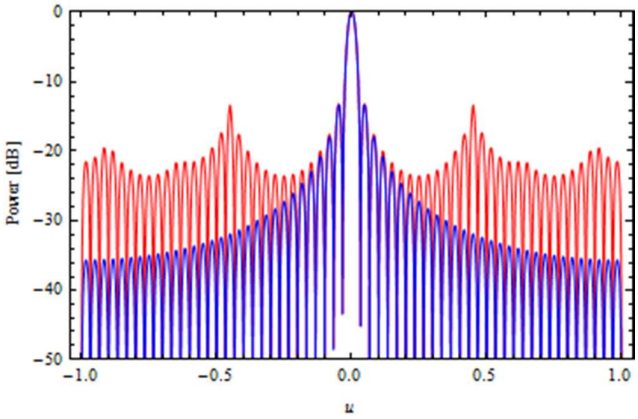

Fig. 3. *In red the pattern of the min-detected coprime array for N=4, M=5, and c=3 (i.e. 24 elements) is reported, compared with that of the ULA with 60 elements, in blue*

However, the patterns reported in Figs. 2 and 3 are not suitable to highlight the actual behaviour of the two detectors in presence of multiple interfering signals. A more effective analysis is based on the evaluation of the scanned responses of the two coprime sub-arrays, defined as

$$s_1(u;t) = \int_{-1}^{1} f_1(u-u')i(u';t)du' + n_1(t) \quad (4)$$

$$s_2(u;t) = \int_{-1}^{1} f_2(u-u')i(u';t)du' + n_2(t) \quad , \quad (5)$$

where t is the time variable, $i(u;t)$ is the input signal (typically, a linear combination of one or more Dirac delta pulses, representing signal sources from different directions), and $n_1(t)$ and $n_2(t)$ represent thermal noise, whose statistical characterization is discussed in Appendix A. This analysis will be reported in Section III, where relevant drawbacks of the min detector will be unveiled and a new processing strategy for coprime arrays will be proposed. Performances of the proposed and available detectors in terms of grating lobe rejection, PSLR and ISLR, thermal noise rejection, accuracy of estimation of received power, PoD and FAR for different SNR values will be also analysed.

3. Proposed processor and experimental results

3.1. "Ghost target" problem and proposed processor

The min detector described in the previous section experiences relevant problems whenever multiple interferers arrive from the directions of the grating lobes of both sub-arrays simultaneously. More specifically, when two input signals are present, one arriving from one of the grating lobes of the first sub-array and the other from one of the grating lobes of the second sub-array, they will give rise to "ghost" targets: the min detector's output signal will be high for some directions in which no source is actually present. To illustrate this, let us consider a coprime array with N=4, M=5, and c=3, which is made up of 24 elements. According to (3), the considered coprime array has a TF=0.6. In addition, let us assume that the input signal

$$i(u;t) = i_{0.5}(t)\delta(u-0.5) + i_{0.4}(t)\delta(u-0.4) \tag{6}$$

is composed of two uncorrelated sources $i_{0.5}$ and $i_{0.4}$ presenting a complex circular Gaussian probability density function (pdf), $\delta(\cdot)$ being the Dirac delta. The first source arrives from u=0.5 with power 0 dB, whereas the other one arrives from u=0.4 and has power −3 dB. Appropriate noise is considered according to (4) and (5) (see Appendix A), with sensor level SNR (i.e., the SNR as measured for a single array element) equal to 0 dB with respect to the weakest source. Once s_1 and s_2 are obtained via (4) and (5), we implement the min detector as

$$s_{out} = \min\{\langle|s_1|^2\rangle_T, \langle|s_2|^2\rangle_T\}\ , \tag{7}$$

where $|\cdot|$ stands for modulus and $\langle\cdot\rangle_T$ represents a temporal average over a time span T. In particular, the temporal average is performed considering 50 signal snapshots. The obtained result is reported in red in Fig. 4*a*. Similarly, in Fig. 4*a* we report in green (partly masked by the superposed blue line, see below) the scanned response of the product detector, implemented as

$$s_{out} = |\langle s_1 s_2^* \rangle_T| \quad , \tag{8}$$

where * stands for complex conjugate. In Fig. 4*b* the response of the corresponding ULA made up of 60 elements is reported as a reference. It is evident that for the min detector two "ghost" targets with power equal to $\langle |i_{0.4}|^2 \rangle_T$ (i.e., −3 dB) can be appreciated in u=0 and u=0.9. Conversely, with regard to the product detector, being the two sources uncorrelated, the "ghost" targets are not present; however, in several directions the sidelobe peak levels are higher than those of the min detector.

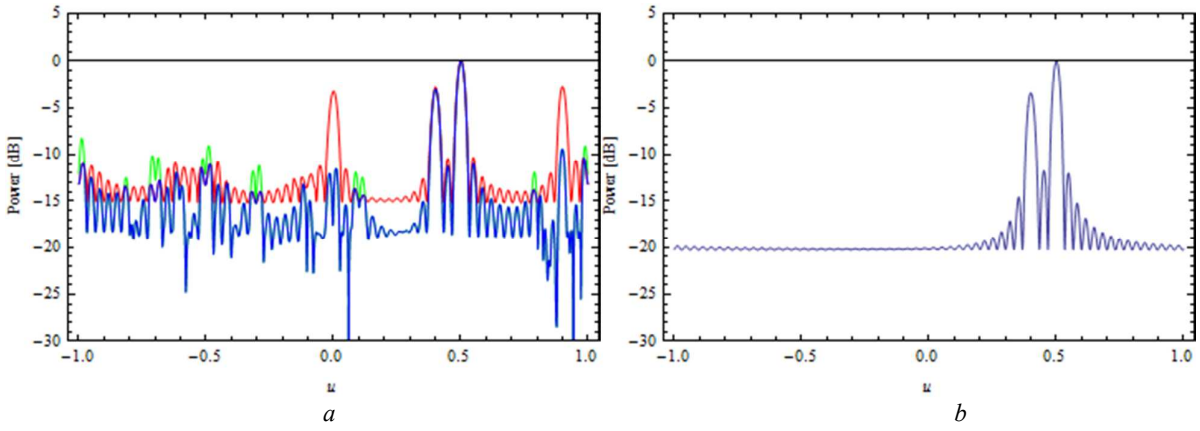

Fig. 4. *Scanned responses with sources located at u=0.4 and u=0.5*

a Product detector (green), min detector (red), and proposed detector (blue)

b Corresponding ULA

Based on the above discussion, in order to maintain the "ghost rejection" property of the product detection, while preserving the low sidelobe level of the min detector, we suggest the architecture schematized in Fig. 5. In particular, the output of the proposed processor s_{out} is given by

$$s_{out} = \min\{\langle |s_1|^2 \rangle_T, \langle |s_2|^2 \rangle_T, |\langle s_1 s_2^* \rangle_T|\} \quad . \tag{9}$$

The scanned response obtained with the proposed processor for the above-discussed case, reported in blue in Fig. 4*a*, testifies that no "ghost" targets are present, similarly to the product detector, and, at the same time, sidelobe levels are never higher than those of the min and product detectors.

We explicitly note that in the ULA scanned response an about −20 dB noise floor is present, in agreement with eq. (17) of Appendix A, whereas for the min detector the noise floor is at about −15 dB. Conversely, both the product detector, and, consequently, the proposed one, are able to partly reject the noise, reaching a noise floor almost equal to the ULA one, as shown by their scanned responses. This is due to the fact that n_1 and n_2 are almost uncorrelated, as explained in Appendix A.

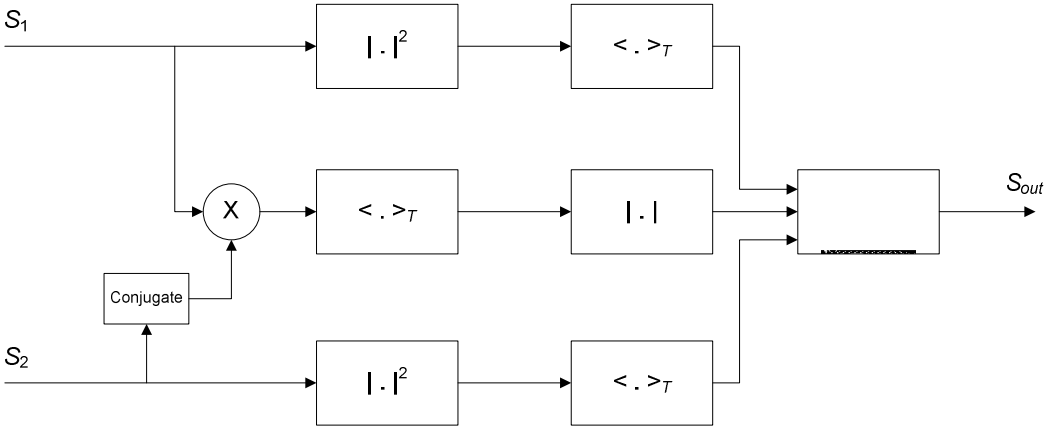

Fig. 5. *Block diagram of the proposed processor*

3.2. Comparison of detectors' scanned responses

Let us now compare the proposed and available detectors performances in terms of PSLR and ISLR. With this aim, we consider the scanned responses obtained in presence of a single source

$$i(u;t) = i_0(t)\delta(u) \quad , \tag{10}$$

where i_0 arrives from broadside, and has the same statistics of $i_{0.5}$ in the previous example. In the absence of thermal noise, the scanned responses for the product and min detectors are coincident with the patterns of Figs. 2*b* and 3 (red lines), respectively, and the proposed detector's scanned response is perfectly coincident with the min detector's one. Therefore, in this case the proposed detector shares the min detector advantage in terms of PSLR. In the presence of noise, with sensor level SNR=0 dB, we obtain the

scanned responses shown in Fig. 6*a* for product, min, and proposed detectors. In Fig. 6*b* the scanned response of the corresponding ULA is shown as a reference. Visual inspection of graphs of Fig. 6*a* shows that the proposed detector outperforms the other two detectors in terms of both PSLR and ISLR. This is quantitatively confirmed by the PSLR values reported in Table 1. In fact, in this case, the proposed detector shows both the low sidelobe property of the min detector, and the noise rejection property of the product detector.

The advantage of the proposed detector in terms of lower sidelobes is shown also in the case analyzed in Fig. 7, where

$$i(u;t) = i_0(t)\delta(u) + i_{0.5}(t)\delta(u-0.5) \quad , \tag{11}$$

i.e. two uncorrelated sources are present: one arriving from u=0.5 with power 0 dB and the other one from broadside with power −3 dB. Appropriate noise with sensor level SNR=0 dB with respect to the weakest source is considered. In this case, the two sources are correctly identified by all the detectors, but the proposed one presents significantly lower sidelobe levels.

Table 1 PSLR of different detectors for N=4, M=5 and c=3, and PSLR of the corresponding ULA.

	PSLR [dB] No noise	PSLR [dB] Sensor level SNR = 0 dB
Product detector	10	7.5
Min detector	13	9
Proposed detector	13	10
ULA	13	12

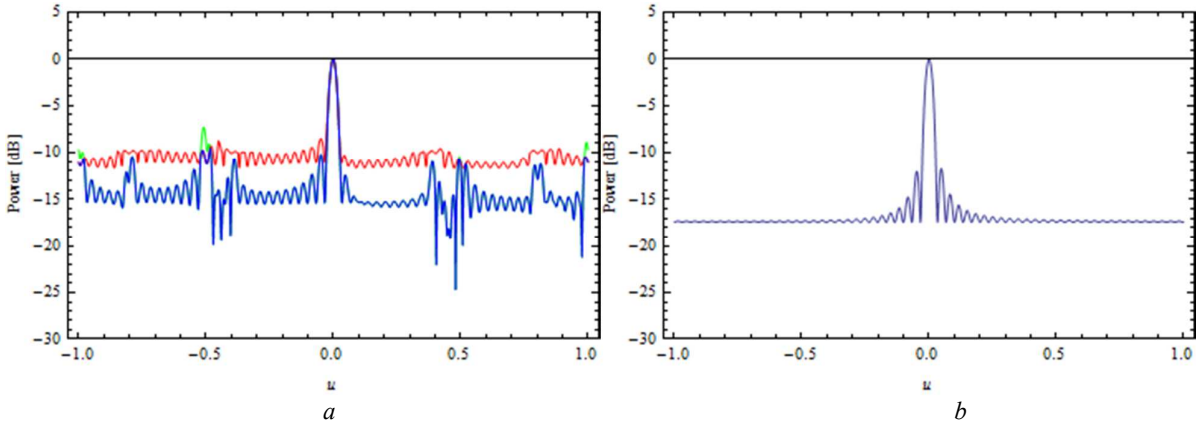

Fig. 6. *Scanned responses with source located at broadside*

a Product detector (green), min detector (red), and proposed detector (blue)

b Corresponding ULA

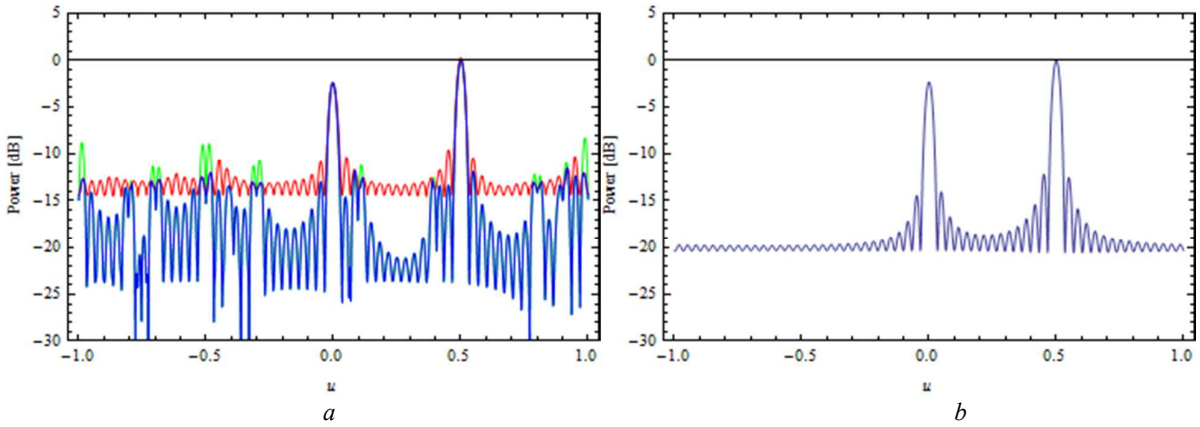

Fig. 7. *Scanned responses with sources located at broadside and u=0.5*

a Product detector (green), min detector (red), and proposed detector (blue)

b Corresponding ULA

Finally, let us consider one last scenario that allows us to compare the detectors' accuracies in terms of measured signal power level. The results relevant to this scenario are reported in Fig. 8. Here we assume the presence of three uncorrelated sources

$$i(u;t) = i_0(t)\delta(u) + i_{0.4}(t)\delta(u-0.4) + i_{0.5}(t)\delta(u-0.5) \quad , \qquad (12)$$

with i_0 and $i_{0.4}$ having power −3 dB and $i_{0.5}$ 0 dB. Appropriate noise is considered, with sensor level SNR=0 dB with respect to the weakest sources. In this case, the advantage of using the proposed detector

is evident. Indeed, with respect to the product detector the sidelobe level is significantly lower. The min detector, similarly to the situation of Fig. 4, gives rise to one "ghost" target for u=0.9 with power equal to $\langle|i_0|^2\rangle_T$ (i.e., –3 dB); moreover, due to the presence of the interfering sources, it is not able to recover the correct amplitude level of the target arriving from broadside. In particular, the power of this target is overestimated of more than 3 dB. This is due to the fact that in this situation the output of the min detector when the array is pointed at broadside will be (by neglecting the very small noise term)

$$s_{out} = \min\{\langle|s_1|^2\rangle_T, \langle|s_2|^2\rangle_T\} = \min\{\langle|i_0 + i_{0.5}|^2\rangle_T, \langle|i_0 + i_{0.4}|^2\rangle_T\} \quad . \tag{13}$$

In the specific case study considered in Fig. 8, the power received from broadside will be equal to $2\langle|i_0|^2\rangle_T$, i.e. twice the power of the lowest-power source located at broadside. Conversely, for the product detector we have

$$s_{out} = |\langle s_1 s_2^*\rangle_T| = \langle(i_0 + i_{0.5})(i_0 + i_{0.4})^*\rangle_T = \langle|i_0|^2\rangle_T \quad , \tag{14}$$

which is the correct estimate of the power coming from broadside, and is also the estimate of the proposed detector. This demonstrates that, while in general the product and proposed detectors provide correct power estimation, conversely, in some critical situations, the min detector provides overestimated power estimates, due to the influence of interfering sources.

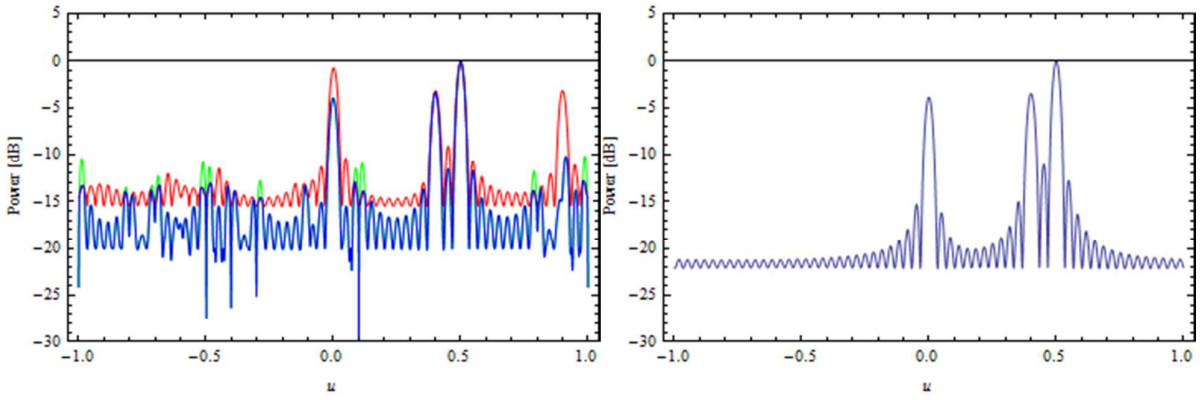

a b

Fig. 8. *Scanned responses with sources located at broadside, u=0.4 and u=0.5*

a Product detector (green), min detector (red), and proposed detector (blue)

b Corresponding ULA

3.3. Comparison of detectors' ROC curves

We want now to compare the different detectors in terms of PoD and FAR. An efficient way of doing this is to compute the detectors' receiver operating characteristic (ROC) curves, which provide, for each value of the FAR, the corresponding value of PoD. As in the previous subsections, target, noise and, when present, interferers are modelled as independent complex random signals with circular Gaussian pdf, and correlation properties of noises $n_1(t)$ and $n_2(t)$ are those discussed in Appendix A. PoD and FAR values are computed via Monte Carlo simulations, by using 1 million realizations of each detector output.

In Fig. 9 we show the ROC curves obtained under the assumption that no interferer is present. Time averages in (7)-(9) are performed considering 5 signal snapshots. We considered sensor level SNR values equal to −6 dB (Fig. 9*a*), 0 dB (Fig. 9*b*), and 6 dB, but the ROC curves of the last case are not shown because, in the range of simulated FAR values, PoD is practically unitary for all the detectors. For all SNR values, product and proposed detectors perform better than the min detector, due to the noise suppression property implied by the correlation operation in presence of almost uncorrelated noises on the two subarrays.

The abovementioned situation changes if we consider the presence of a single interferer placed at a random position. In particular, we assume that one interferer is present, with sensor level interferer-to-noise ratio (INR) equal to 3 dB, and whose position u_0 is a uniform random variable in the interval −1 to 1, excluding the mainlobe. Again, time averages in (7)-(9) are performed considering 5 signal snapshots. Corresponding ROC curves are shown in Figs. 10*a*, 10*b*, and 10*c* for sensor level SNR values equal, again, to −6 dB, 0 dB, and 6 dB, respectively. In this case, due to the lower sidelobe level of min and proposed detectors, the latter show better performances with respect to the product detector (actually, for the lowest SNR value, all the detectors perform quite poorly).

Finally, we consider the very critical situation of the presence of two interferers, one arriving from one of the grating lobes of the first sub-array and the other from one of the grating lobes of the second sub-array. In particular, we consider an interferer placed at u=0.4, with sensor level INR equal to 0 dB, and an interferer placed at u=0.5, with sensor level INR equal to 3 dB. In addition, time averages in (7)-(9) are performed considering 50 signal snapshots. Corresponding ROC curves are shown in Figs. 11*a*, 11*b*, and 11*c* for sensor level SNR values equal to −3 dB, 0 dB, and 3 dB, respectively. In this case, apart from the lowest SNR value, for which all detectors show similar poor performances, product and proposed detectors show better performances with respect to the min detector. This is motivated by the fact that, as

we showed in the previous subsections, in this particular situation the min detector is subject to the appearance of "ghost" targets, which increase its FAR.

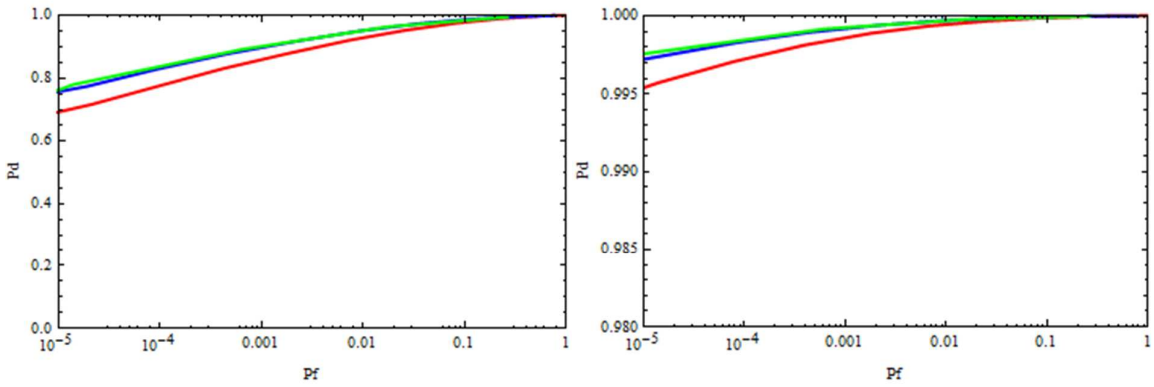

a *b*

Fig. 9. *ROC curves in absence of interferers: product detector (green), min detector (red), and proposed detector (blue)*

a Sensor level SNR= −6 dB

b Sensor level SNR= 0 dB

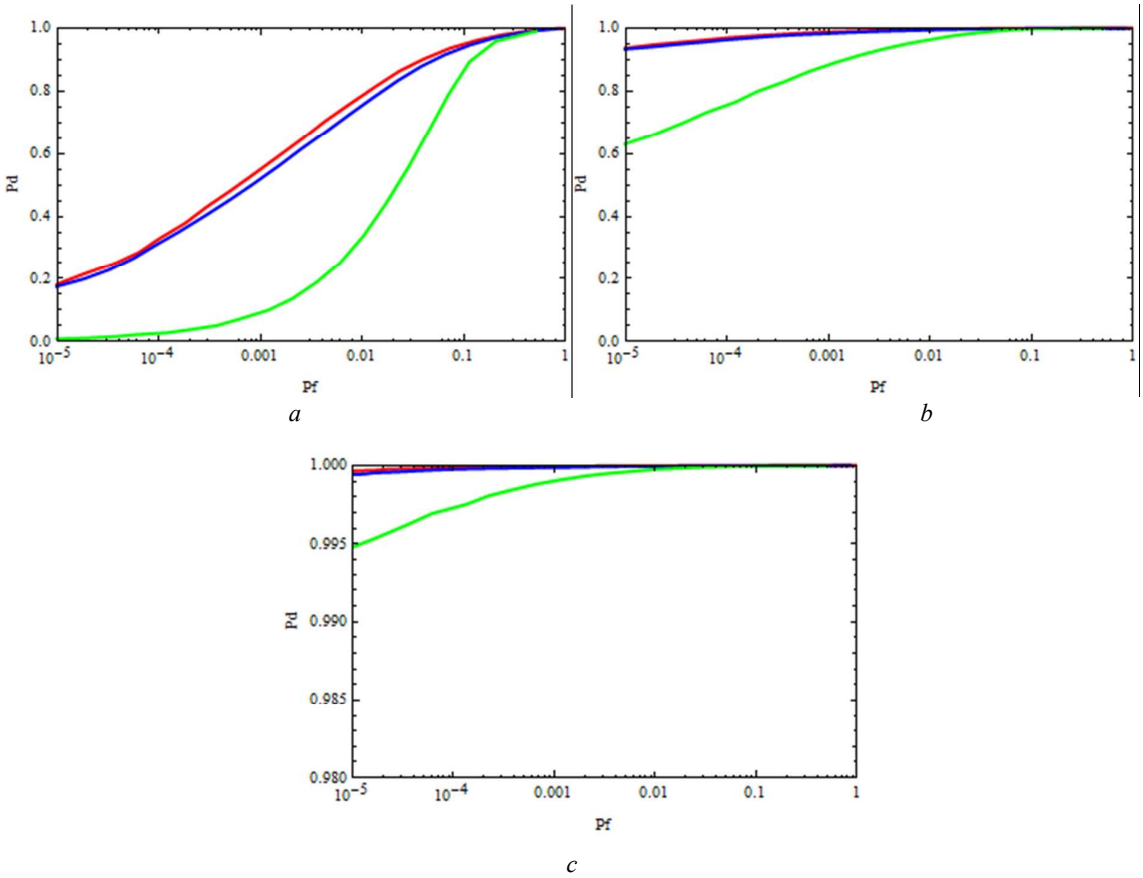

a *b*

c

Fig. 10. *ROC curves in presence of one interferer with random location: product detector (green), min detector (red), and proposed detector (blue)*

a Sensor level SNR=–6 dB

b Sensor level SNR=0 dB

c Sensor level SNR=6 dB

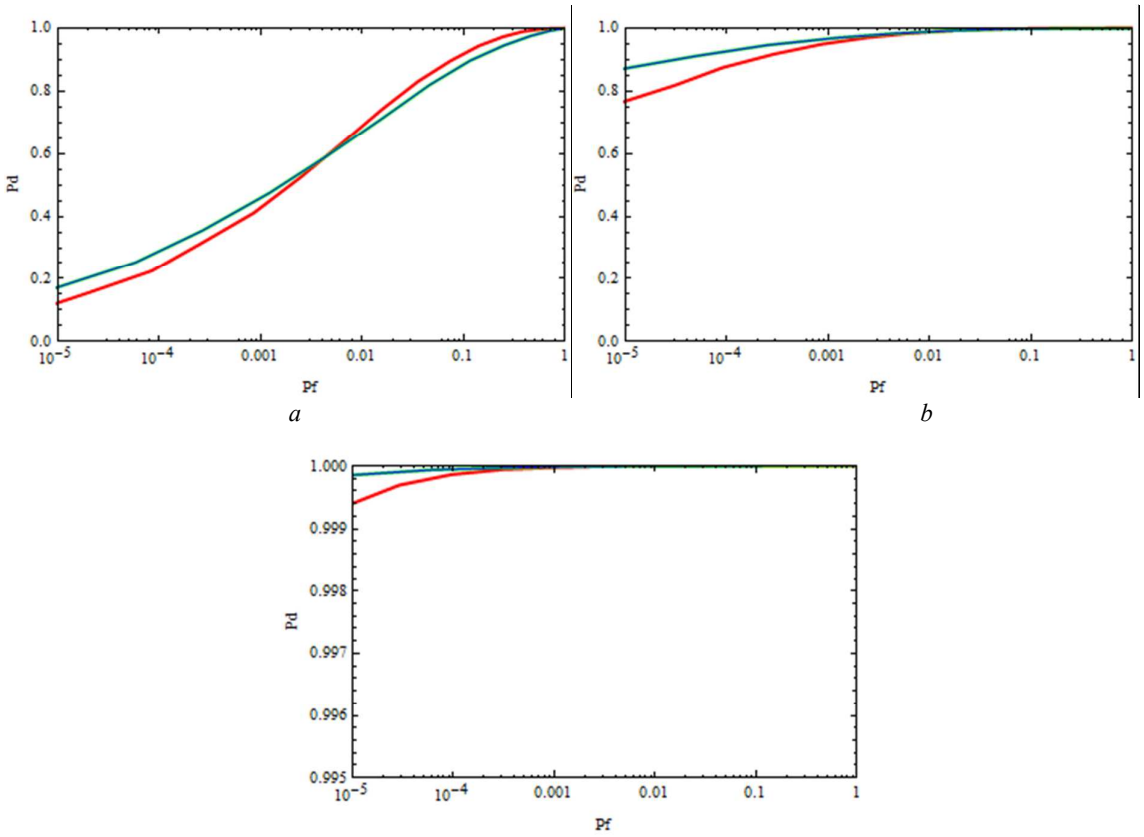

Fig. 11. *ROC curves in presence of interferers located at u=0.4 and u=0.5: product detector (green), min detector (red), and proposed detector (blue)*

a Sensor level SNR=–3 dB

b Sensor level SNR=0 dB

c Sensor level SNR=3 dB

3.4. Summary and discussion of results

Presented results can be summarized by stating that in all cases the proposed detector performs as the better one between product and min detectors. More in detail, the product detector shows noise-

rejection properties, so that, in terms of PoD and FAR, it performs better than the min detector in the absence of interferers; in addition, the product detector shows ghost-rejection properties, so that it performs better than the min detector, both in terms of PoD and FAR, and in terms of measured power level accuracy, in the presence of two interferers placed in particular positions that give rise to "ghost targets" in the min detector. On the other hand, the min detector has lower sidelobes, so that it performs better than the product detector in terms of PSLR and also in terms of PoD and FAR when a single interferer is present. Finally, the proposed detector shows both noise-rejection and ghost-rejection properties, as the product detector, and low sidelobe level, as the min detector, so that it always performs as the better one of the two already available detectors.

4. Conclusion

Coprime arrays represent a convenient sparse configuration, due to the high attainable TFs. They are particularly suitable for active and passive beamforming applications, such as radar. However, the processing strategies available in the literature for the combination of the signals received by the two sub-arrays suffer from high PSLR and ISLR, and, in some critical situations, i.e. in presence of multiple interfering sources, from the appearance of "ghost" targets.

In this paper, we have proposed a new detector that solves the problems of the standard product and min detectors, inheriting the benefits of both of them, without the associated drawbacks. In particular, we demonstrated its use in several canonical situations, in presence of multiple interfering sources and additive noise. The simulated scanned responses and ROC curves testify the ability of the proposed processor to cope with situations that are critical for the other detectors. In particular, it solves the problem of "ghost" targets and attains, by definition, the minimum PSLR and ISLR. In addition, it maintains the noise-rejection property of the product detector.

As a final remark, we want to highlight that the proposed processing can be attractive also for active beamforming radar applications, at least for the case of pulsed radars. In this case, usually one of the two sub-arrays is used in transmission and the other one in reception. Doing so, the receiving array does not see the grating lobes of the transmitting one and the output signal is reconstructed without the need of further processing [1]. However, in situations in which the presence of jamming signals is possible, the receiving sub-arrays may still receive "ghost" targets, whenever the jammer is arriving from the receiver's grating lobes. In these situations, we suggest to use both arrays in reception in order to apply to the received signals the processing proposed in this paper, which is able to assure jammer rejection and sidelobe levels' reduction.

Appendix A

Let us consider a uniform array of L receiving elements (or "sensors"), each one connected to an independent receiver, so that it is possible to access the individual signals received by each sensor, as it is usual in modern beamforming radar and AoA applications. We model noises affecting different sensors as independent identically distributed zero-mean, σ_n^2-variance complex random processes with circular Gaussian pdf. Similarly, we model the signal to be detected (i.e., the source signal), arriving from a given direction, as a zero-mean, σ_s^2-variance complex random process with circular Gaussian pdf. Accordingly, the SNR at each array element, which we name "sensor level SNR" (SNR_{sl}), is σ_s^2/σ_n^2. When the scanned direction coincides with the source direction, the array processing weights the signals received by the different sensors in such a way that the copies of source signal are all in-phase and sum up coherently. Conversely, noises at different sensors are independent and then they sum up incoherently. Accordingly, the SNR at the output of the array processing, which we name "output SNR", is increased by a factor L with respect to the sensor level SNR, so that it is equal to $L\sigma_s^2/\sigma_n^2$.

By applying above results to the two subarrays of a coprime array and to the corresponding ULA, we obtain that the output SNR of subarray 1, subarray 2, and ULA are, respectively:

$$SNR_1 = cM\ SNR_{sl} = cM\ \sigma_s^2/\sigma_n^2 \quad , \tag{15}$$

$$SNR_2 = cN\ SNR_{sl} = cN\ \sigma_s^2/\sigma_n^2 \quad , \tag{16}$$

$$SNR_{ULA} = cMN\ SNR_{sl} = cMN\ \sigma_s^2/\sigma_n^2 \quad . \tag{17}$$

It is important to note that the output noises $n_1(t)$ and $n_2(t)$ are partly correlated, because the two subarrays share c elements (out of cM for subarray 1, and out of cN for subarray 2). It is easy to verify that the correlation coefficient of n_1 and n_2 is

$$\rho = \frac{E(n_1 n_2^*)}{\sqrt{E(|n_1|^2)E(|n_2|^2)}} = \frac{1}{\sqrt{NM}} \quad , \tag{18}$$

where $E(\cdot)$ stands for statistical mean. This coefficient is low, so that noises over the two subarrays are almost uncorrelated. It also turns out that, under ergodicity assumption, if the product detector uses a very (ideally, infinitely) long averaging interval T, its final SNR is equal to the ULA one:

$$SNR_{prod} = \frac{\sigma_s}{E(\langle n_1 n_2^* \rangle_T)} \underset{T\to\infty}{\longrightarrow} \frac{\sigma_s}{E(n_1 n_2^*)} = \frac{\sigma_s cMcN}{c\sigma_n} = cMN\ SNR_{sl} = SNR_{ULA} \quad . \tag{19}$$

For finite T, the time averaged correlation is always greater than the statistical one, so that in practice the product detector final SNR never attains the ideal SNR_{ULA} value. However, an appreciable noise rejection is obtained by the product detector due to time averaging, as verified in the numerical results of Section 3.

5. References

[1] Vaidyanathan, P. P., Pal, P.: 'Sparse Sensing With Co-Prime Samplers and Arrays', IEEE Trans. Signal Process., 2011, **59**, (2), pp. 573–586

[2] Vaidyanathan, P. P., Pal, P.: 'Theory of Sparse Coprime Sensing in Multiple Dimensions', IEEE Trans. Signal Process., 2011, **59**, (8), pp. 3592–3608

[3] Adhikari, K., Buck, J. R., Wage, K. E.: 'Extending coprime sensor arrays to achieve the peak side lobe height of a full uniform linear array', EURASIP J. Adv. Signal Process., 2014, **2014**, (148), pp. 1–17

[4] Qin, S., Zhang, Y. D., Amin, M. G.: 'Generalized Coprime Array Configurations for Direction-of-Arrival Estimation', IEEE Trans. Signal Process., 2015, **63**, (6), pp. 1377–1390

[5] Tan, Z., Eldar, Y. C., Nehorai, A.: 'Direction of Arrival Estimation Using Co-Prime Arrays: A Super Resolution Viewpoint', IEEE Trans. Signal Process., 2014, **62**, (21), pp. 5565-5576

[6] Qin, S., Zhang, Y. D., Amin, M. G.: 'Generalized coprime array configurations', Proc. 8th IEEE Sensor Array and Multichannel Signal Processing Workshop (SAM), A Coruna, Spain, June 2014, pp. 529-532

[7] Di Martino, G., Iodice, A.: 'Coprime Synthetic Aperture Radar (CopSAR): A New Acquisition Mode for Maritime Surveillance', IEEE Trans. Geosci. Remote Sens., 2015, **53**, (6), pp. 3110–3123

[8] Liu Y., Buck, J. R.: 'Detecting Gaussian Signals in the Presence of Interferers Using the Coprime Sensor Arrays with the Min Processor'. Proc. Asilomar Conf., Pacific Grove, USA, November 2015, pp. 370–374

[9] Hoctor, R. T., Kassam, S. A.: 'The Unifying Role of the Coarray in Aperture Synthesis for Coherent and Incoherent Imaging', Proc. IEEE, 1990, **78**, (4), pp. 735–752

[10] Krieger, J. D., Kochman, Y., Wornell, G. W., 'Multi-Coset Sparse Imaging Arrays', IEEE Trans. Antennas Propag., 2014, **62**, (4), pp. 1701–1715

[11] Mailloux, R. J.: Phased Array Antenna Handbook (Artech House, 2nd edn. 2005)

[12] Howland, P.: 'Editorial: Passive radar systems', IEE Proc., Radar Sonar Navig., 2005, **152**, (3), pp. 105-106

[13] Griffiths, H. D., Baker, C. J., 'Passive coherent location radar systems. Part 1: performance prediction', IEE Proc., Radar Sonar Navig., 2005, **152**, (3), pp. 153-159

[14] Di Martino, G., Iodice, A.: 'Orthogonal Coprime Synthetic Aperture Radar', IEEE Trans. Geosci. Remote Sens., 2016, in print (available online, doi: 10.1109/TGRS.2016.2608140)